Solid State Communications 408 (2026) 116227

Contents lists available at ScienceDirect

Solid State Communications

journal homepage: www.elsevier.com/locate/ssc

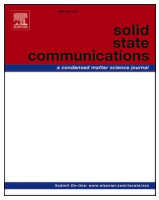

Electronic, magnetic, mechanical and optical properties of CoCrZrAl and RuCrZrGa quaternary Heusler alloys

I. Bensehil [a,b], H. Baaziz [c,d,*], T. Ghellab [c,d], Z. Charifi [c,d]

[a] Faculty of Technology, University of M'sila, University Pole, Road Bordj Bou Arreridj, M'sila, 28000, Algeria
[b] Laboratory of Surfaces and Interfaces Studies of Solid Materials, University of Setif 1, Algeria
[c] Department of Physics, Faculty of Science, University of M'sila, 28000, M'sila, Algeria
[d] Laboratory of Physics and Chemistry of Materials, University of M'sila, Algeria

ARTICLE INFO

Communicated by: Luis Brey

Keywords:
Quaternary Heusler alloys
Half-metallicity
Spintronic applications
Elastic properties
Optical properties

ABSTRACT

This study employs first-principles density functional theory (DFT) calculations within the GGA-PBEsol framework to comprehensively investigate the structural, elastic, electronic, magnetic, and optical properties of CoCrZrAl and RuCrZrGa quaternary Heusler alloys. Both compounds are found to be stable in the ferromagnetic Y-III phase with equilibrium lattice constants of 6.19 Å and 6.24 Å, respectively. Electronic structure calculations reveal a half-metallic character, exhibiting 100 % spin polarization at the Fermi level with minority spin band gaps of 1.18 eV for CoCrZrAl and 1.19 eV for RuCrZrGa. The total magnetic moments are 4 μB and 3 μB, in full agreement with the Slater-Pauling rule. Mechanical property analysis confirms their ductile nature and elastic stability. Furthermore, optical properties, including a high absorption coefficient in the visible and ultraviolet regions, suggest significant potential for optoelectronic applications. These results position CoCrZrAl and RuCrZrGa as promising candidates for advanced spintronic and optoelectronic devices.

1. Introduction

Half-metallic ferromagnetic materials are a distinct class of compounds characterized by the ability to exhibit metallic conductivity for electrons of one spin orientation, while acting as semiconductors or insulators for the opposite spin orientation. This phenomenon, which was first theoretically predicted by Groot et al. in 1983 [1], represents a significant breakthrough in condensed matter physics and has profound implications for spintronic applications, where efficient spin injection and manipulation are paramount [2]. The discovery of half-metallic ferromagnetism has since driven extensive research into materials that exhibit this property, particularly focusing on compounds that offer near-100 % spin polarization at the Fermi level, a critical feature for the development of high-performance spintronic devices such as magnetic sensors, data storage systems, and thermoelectric devices [3–5].

Among these materials, quaternary Heusler alloys (QHAs), which are represented by the formula XX'YZ (where X, X′, and Y are transition metals and Z is a main group element), have gained considerable attention due to their unique properties and tunability. These alloys extend the well-studied ternary Heusler compounds, which have been investigated for more than a century, and offer a high degree of flexibility in terms of their electronic structure, magnetic properties, and half-metallic behavior. By varying the constituent elements and adjusting the atomic ordering within the crystal structure, it is possible to precisely control the materials' spin polarization, magnetic moments, and other key properties. This tunability makes QHAs especially attractive for spintronic applications, where high spin polarization and stability at room temperature are essential [6–9].

Quaternary Heusler alloys typically crystallize in the cubic F43m space group (N.216), a symmetry that facilitates both high spin polarization and strong magnetic ordering, often persisting at room temperature. The fundamental electronic characteristic of half-metallic ferromagnets lies in their electronic band structure: one spin channel exhibits metallic conductivity, while the opposite spin channel is either insulating or semiconducting, leading to nearly complete spin polarization at the Fermi level [10,11]. This spin polarization is a key factor in enabling efficient spin transport, and thus, these materials are particularly suited for devices such as magnetic tunnel junctions and spin filters, where high spin polarization is a requirement for optimal performance.

Quaternary Heusler alloys have garnered significant interest for their remarkable magnetic, electronic, thermoelectric, and mechanical

* Corresponding author. Department of Physics, Faculty of Science, University of M'sila, 28000, M'sila, Algeria.
E-mail addresses: baaziz_hakim@yahoo.fr, hakim.baaziz@univ-msila.dz (H. Baaziz).

https://doi.org/10.1016/j.ssc.2025.116227
Received 17 September 2025; Received in revised form 1 November 2025; Accepted 6 November 2025
Available online 12 November 2025

properties, making them prime candidates for advanced technologies in spintronics, energy harvesting, and optoelectronics. Their suitability for spintronics is demonstrated by alloys like CoFeXSn (X = Ru, Zr, Hf, Ta) and MCrTaM' (M = Fe, Ru; M' = Al, Ga, Si, Ge), which are half-metallic ferromagnets (HMF). This characteristic provides 100 % spin polarization, which is essential for generating the highly spin-polarized currents required in advanced spintronic devices [12,13]. Furthermore, these alloys show great promise for sustainable energy applications, as evidenced by the notable thermoelectric efficiency of CoRuCrSi, which achieves a ZT value of 0.43 at 400K [14]. The promise of Co- and Ru-based quaternary Heusler alloys is further demonstrated by systems like CoRuMnZ, which show high spin polarization and remarkable resilience to atomic disorder, maintaining half-metallicity even in non-ideal structures [15]. This robustness is critical for practical device fabrication. Building on these findings, we investigate the novel compounds CoCrZrAl and RuCrZrGa to explore their potential for achieving perfect 100 % spin polarization and enhanced stability, thereby expanding the family of viable spintronic materials.

Recent theoretical and experimental studies have contributed significantly to the understanding of the structural, electronic, magnetic, optical, and mechanical properties of quaternary Heusler alloys. For example, Khadhraoui et al. [16] explored the CoFeYGe system (with Y = Hf, Ta), demonstrating that both alloys exhibit half-metallic ferromagnetism with indirect band gaps of 1.46 eV for CoFeHfGe and 0.77 eV for CoFeTaGe, making them promising candidates for spintronic applications. Similarly, Masri et al. [17] showed that FeMnScAl is a half-metal, exhibiting a narrow band gap of 0.677 eV, along with high refractive indices and substantial ultraviolet absorption, suggesting its potential in photovoltaic and optoelectronic devices. Prakash et al. [18] studied FeCrYZ alloys (Y = Ti, Zr, Hf; Z = Sn, Sb) and found that they exhibit 100 % spin polarization at the Fermi level, narrow band gaps, and excellent thermoelectric performance, which further underscores their suitability for both spintronic and optoelectronic applications. Xiao-Ping Wei [19] investigated the structural, magnetic, and electronic properties of CrZrCoZ (Z = Al, Ga, In, Tl, Si, Pb), revealing that these alloys are half-metallic ferrimagnets with Curie temperatures significantly exceeding room temperature, further enhancing their prospects for high-temperature spintronic applications. RuMnCrSi [20], which exhibits half-metallic ferrimagnetism with a band gap of 0.806 eV in the majority spin channel, also shows strong ultraviolet absorption, making it a good candidate for both spintronic devices and ultraviolet photodetectors.

In addition to their half-metallic characteristics [21–26], many QHAs exhibit semiconductor-like behavior under certain conditions [27–29], adding a layer of complexity and functionality. This dual behavior makes these materials particularly attractive for applications that require both metallic and semiconducting properties, such as magnetic tunnel junctions or spin-based transistors. The combination of these properties allows for a new class of devices that can exploit the full potential of spin-polarized transport.

The primary goal of this work is to perform a detailed and rigorous investigation into the structural, electronic, magnetic, optical, and elastic properties of quaternary Heusler alloys. This study seeks to explore how these properties interrelate and how they contribute to the material's half-metallic behavior, while also examining their potential for spintronic and optoelectronic applications. Specifically, the objectives are to: (1) elucidate the role of crystal symmetry and atomic ordering in influencing the electronic structure and magnetic properties; (2) examine the impact of compositional variations on spin polarization and band gap characteristics; (3) explore the optical properties such as refractive index and absorption spectrum, with a focus on potential applications in light-based technologies; (4) investigate the mechanical and elastic properties to assess the stability and robustness of these alloys under practical conditions. This comprehensive analysis aims to provide a deeper understanding of the underlying mechanisms that govern the half-metallic behavior of these materials, and to ultimately enable the design and optimization of quaternary Heusler alloys for high-performance spintronic and optoelectronic devices.

Table 1
Three different occupying positions of XCrZrZ quaternary Heusler alloys in the Y-Type structures.

	4a (0,0,0)	4c (1/4, 1/4, 1/4)	4b (1/2, 1/2, 1/2)	4d (3/4, 3/4, 3/4)
YI	**Z**	**X**	**Cr**	**Zr**
YII	**Z**	**Cr**	**X**	**Zr**
YIII	**X**	**Z**	**Cr**	**Zr**

2. Computational details

The crystalline structure, elasticity, electronic transitions, and magnetic properties of Heusler alloys were analyzed using spin-polarized calculations. These computations were performed with the pseudopotential plane-wave method, as implemented in the CASTEP code [30,31]. The exchange-correlation functional was approximated using the generalized gradient approximation (GGA-PBEsol) [32], and an ultrasoft Vanderbilt-type pseudopotential was employed to describe the interaction between valence electrons and the core [33]. The electronic configurations for the elements involved were: [Co] = [Ar] $4s^2$ 3 d^7, [Cr] = [Ar] $4s^1$ 3 d^5, [Zr] = [Kr] $5s^2$ 4 d^2, [Al] = [Ne] $3s^2$ $3p^1$, [Ru] = [Kr] $5s^1$ 4 d^7, and [Ga] = [Ar] 3 d^{10} $4s^2$ $4p^1$. For geometry optimization, Brillouin zone integration was conducted using a 14 × 14 × 14 k-point grid, with a plane-wave cutoff energy of 450 eV. The convergence criterion for the self-consistent field was set to 5×10^{-6} eV/atom to ensure sufficient computational accuracy. The elastic constants (C_{ij}) were computed using the stress-strain approach [34]. Both compounds under study crystallize in a cubic structure. Ground-state properties such as lattice constant (a_0), volume (V_0), bulk modulus (B_0), and its pressure derivative (B'_0) were obtained by fitting the total energy (E) as a function of unit cell volume (V) to the Birch-Murnaghan equation of state [35].

$$E(V) = E_0 + \frac{9}{16}B_0V_0\left(\frac{V}{V_0}\right)^{-\frac{2}{3}}\left[\left(\frac{V}{V_0}\right)^{\frac{2}{3}}-1\right]^2\left[1+\frac{3}{4}(B'_0-4)\left(\left(\frac{V}{V_0}\right)^{\frac{2}{3}}-1\right)\right] \quad (1)$$

The structural stability of the two compounds was evaluated by calculating their formation (E_{For}) energies using the following equation [36]:

$$E_{For} = \frac{1}{4}\left[E^{XCrZrZ}_{Total} - \left(E^{X}_{bulk} + E^{Cr}_{bulk} + E^{Zr}_{bulk} + E^{Z}_{bulk}\right)\right] \quad (2)$$

The formation energy is determined using the equilibrium total energy E^{XCrZrZ}_{Total}, along with the equilibrium total energies per atom for the bulk elements X (Co, Ru), Cr, Zr, and Z (Al, Ga).

3. Results and discussion

This section provides a comprehensive examination of the structural, mechanical, electronic, magnetic, and optical properties of CoCrZrAl and RuCrZrGa alloys, focusing on their fundamental characteristics and performance in various contexts.

3.1. Structural properties

The quaternary Heusler alloys (QHAs) XCrZrZ (X = Co, Ru; Z = Al, Ga) crystallize in the LiMgPdSn-type structure (space group F43m, No. 216), where the 1:1:1:1 stoichiometry permits three distinct structural phases defined by the occupancy of the four Wyckoff positions (Table 1). Our first-principles total energy calculations reveal that the Y-III configuration is the ground state structure for both CoCrZrAl and RuCrZrGa. This structural preference is governed by a minimization of the total energy driven by the optimization of hybridized *d-d* and *d-p*

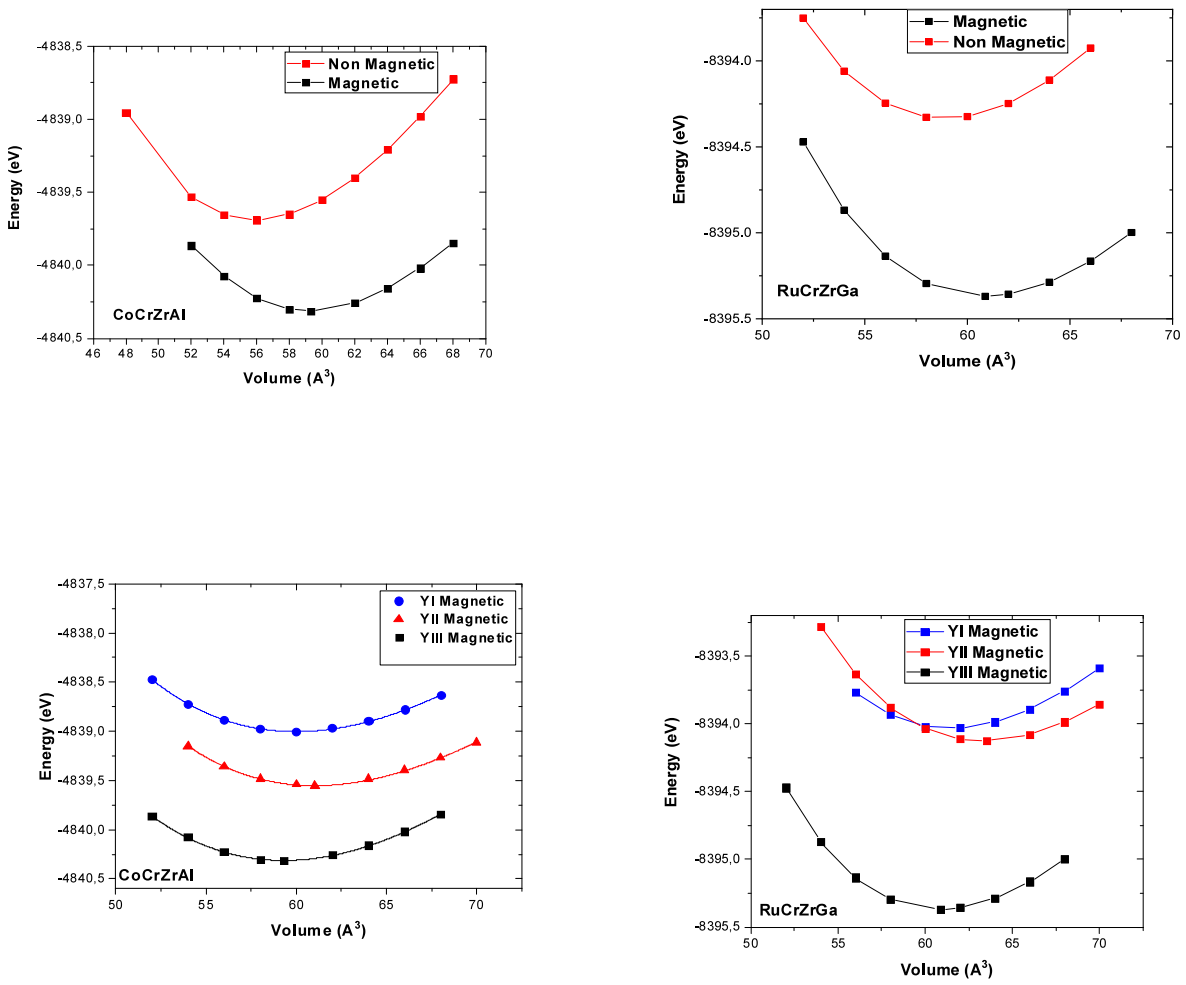

Fig. 1. Total energy as a function of the unit cell volume in the nonmagnetic and magnetic configurations of CoCrZrAl and RuCrZrGa.

Table 2
Calculated equilibrium lattice constant (a_0 (Á)), volume (V_0 (Á^3)), bulk modulus (B (GPa), pressure derivative (B') and formation energy (E_{For}) for CoCrZrAl and RuCrZrGa Heuslers alloys.

Alloys	a_0 (Á)	V_0 (Á^3)	B_0 (GPa)	B'	E_0 (eV)	E_{For} (eV/atom)
CoCrZrAl	6.19, 6.24 [39]	59.301	139.51	2 .47	−4840.3136	−8.20
RuCrZrGa	6.24, 6.32 [39]	60.87	171.19	3.95	−8395.369	−8. 65

bonding networks, placing the Cr atom at the 4b (½, ½, ½) site to maximize favorable exchange interactions, a trend consistent with other magnetic QHAs like CoFeMnZ. The stability of the magnetic state was determined by mapping the total energy as a function of unit cell volume for both non-magnetic (NM) and ferromagnetic (FM) phases (Fig. 1). The FM phase exhibits a pronounced energy lowering across all volumes, with a well-defined parabolic minimum, indicating a stable ferromagnetic ground state. This energy difference, the Stoner gap, arises from the exchange splitting of the electronic states and is a prerequisite for strong magnetism. The depth of the minimum for the FM curve is directly related to the strength of the magneto-volume coupling in these materials.

The equilibrium properties derived from a Murnaghan equation of state fit to the FM E(V) curve are summarized in Table 2. The calculated lattice parameters ($a_0 \approx 6.2$ Å) are consistent with the sum of the metallic radii of the constituent atoms. The bulk modulus B_0, a measure of the crystal's resistance to uniform compression, is significantly higher for RuCrZrGa (171.19 GPa) than for CoCrZrAl (139.51 GPa). This is a direct consequence of the more diffuse and spatially extending Ru *4d* orbitals compared to the more localized Co *3d* orbitals, leading to stronger covalent bonding and a stiffer lattice. The pressure derivative of the bulk modulus, B', which describes the change of B_0 with applied pressure, also differs, suggesting a distinct evolution of the bonding character under hydrostatic stress for the two compounds.

The highly negative formation energies ($E_{For} \sim -8.5$ eV/atom) are a critical result, confirming not just stability but a profound thermodynamic driving force for the formation of these compounds from their elemental constituents. This large energy gain implies a high degree of chemical order and resistance to decomposition, pointing to potentially high melting points and robust phase stability. The combination of structural, energetic, and elastic properties confirms that CoCrZrAl and RuCrZrGa are stable ferromagnets with strong interatomic bonding. The established FM ground state in the Y-III structure provides the essential foundation for probing their electronic structure. The next critical step is to calculate the spin-polarized density of states to evaluate the potential for half-metallicity, where one spin channel is metallic and the other is semiconducting, a property of paramount importance for achieving high spin polarization in spintronic applications such as magnetic tunnel junctions and spin injectors.

3.2. *Elastic properties*

The mechanical properties of materials are paramount in

Table 3
Presently obtained elastic parameters of CoCrZrAl and RuCrZrGa.

Parameters	CoCrZrAl	RuCrZrGa
C_{11}	165.36	246.32
C_{12}	106.12	122.28
C_{44}	84.10	106.05
B	125.87	163.62
G	55. 38	85.52
B/G	2.27	1.91
E	144.88	218.48
σ	0.31	0.28
Θ_D	391.04	420.77
A	1.43	0.35

Table 4
The calculated magnetic moments, *m*(Tot), *m*(Fe), *m*(Y), *m*(Co), *m*(Sb) in μ_B, Band gap (E_g) in eV, and polarization *P* in %.

Alloys	*m*(X)	*m*(Cr)	*m*(Zr)	*m*(Z)	*M*(Tot)	E_g	*P*
CoCrZrAl	**0.81**	**3.04**	**0.08**	**0.07**	**4.00**	**1.18**	**100 %**
RuCrZrGa	**0.05**	**2.89**	**0.04**	**0.02**	**3.00**	**1.19**	**100 %**

determining their behavior under a wide range of mechanical stresses and deformations. These properties are fundamental not only in materials science but also in applications such as structural engineering, advanced manufacturing, and the design of functional devices. Understanding these characteristics allows for the precise selection and optimization of materials to meet specific requirements for performance, reliability, and safety. Among the most critical mechanical properties is the elastic modulus, a key factor in evaluating the material's resistance to deformation under applied forces. The bulk modulus, shear modulus, and Young's modulus are the principal elastic constants that describe how a material responds to uniform compression, shear deformation, and tensile stress, respectively. These parameters are intrinsic to understanding the material's overall mechanical behavior, which influences its suitability for various applications, from structural components to high-performance devices.

In particular, the elastic constants (C_{ij}) form the foundation for exploring the elastic behavior of materials like CoCrZrAl and RuCrZrGa alloys. These constants are fundamental to understanding the response of the material to external forces, as they directly govern the stress-strain relationship within the material. In cubic crystal systems, the elastic constants C_{11}, C_{12}, and C_{14} represent the independent coefficients that characterize the material's resistance to different types of deformation, including longitudinal, lateral, and shear deformations. These constants provide the basis for calculating the material's bulk modulus, shear modulus, and Young's modulus, as well as the material's overall stiffness and strength.

To assess the stability of these cubic crystal structures, the Born-Huang stability criteria [37] offer a rigorous method. This set of criteria is essential for determining the mechanical stability of the material under varying conditions, ensuring that the structure remains stable under external stresses. The criteria are formulated in terms of the elastic constants, and their satisfaction indicates that the material will not undergo structural collapse or phase transitions under normal conditions of stress or strain. These stability conditions are vital in understanding the mechanical integrity of materials in practical applications, as they help predict the material's performance in real-world conditions, including thermal and mechanical loading.

In this context, Table 3 presents the computed values for the elastic constants, moduli, and derived quantities for CoCrZrAl and RuCrZrGa alloys. The accuracy of these values is critical for developing a deeper understanding of how these alloys behave under mechanical stress and how alloying elements affect their elastic properties. The derived quantities, such as the bulk modulus, shear modulus, and Young's modulus, are key indicators of the material's capacity to withstand external deformations without permanent damage. Understanding these values not only aids in material selection but also allows for the fine-tuning of properties to enhance the material's suitability for specific applications, whether in structural, electronic, or other advanced technologies.

$$(C_{11} - C_{12}) > 0;\ (C_{11} + 2C_{12}) > 0;\ C_{11} > 0;\ C_{44} > 0 \text{ and } C_{12} < B < C_{11} \tag{3}$$

Both CoCrZrAl and RuCrZrGa alloys satisfy the Born-Huang stability criteria, indicating that they are elastically stable. This result suggests that these materials will maintain their structural integrity under a wide range of applied stresses, ensuring predictable and stable mechanical behavior across diverse applications. The fulfillment of these stability conditions under external forces implies that the materials will not undergo any undesirable structural transitions or failure modes, which is crucial for their performance in real-world scenarios involving mechanical loading or deformation.

The elastic constants of these alloys provide the necessary foundation to compute various essential elastic parameters that describe the material's response to stress. These include the Young's modulus (E), shear modulus (G), bulk modulus (B), and Poisson's ratio (ν), which characterize the material's ability to resist deformation in different stress regimes. Additionally, the universal anisotropy factor (A^U) can be calculated, providing a quantitative measure of the material's elastic anisotropy. A higher anisotropy factor indicates a greater degree of directional dependence in the material's stiffness, which can influence its behavior under anisotropic loading conditions. To calculate these parameters, the following equations are employed [38]:

$$B = \frac{C_{11} + 2C_{12}}{3} \tag{4}$$

$$G_V = \frac{C_{11} - C_{12} + 3C_{44}}{5} \tag{5}$$

$$G_R = \frac{5(C_{11} - C_{12})C_{44}}{3(C_{11} - C_{12}) + 4C_{44}} \tag{6}$$

$$G_H = \frac{G_V + G_R}{2} \tag{7}$$

$$E = \frac{9BG}{3B + G} \tag{8}$$

$$A^U = 5\frac{G_V}{G_R} + \frac{B_V}{B_R} - 6 \tag{9}$$

$$\sigma = \frac{3B - 2G}{2(3B + G)} \tag{10}$$

The elastic constants C_{11}, C_{12}, and C_{44} form the cornerstone of understanding the mechanical response and bonding characteristics of CoCrZrAl and RuCrZrGa quaternary Heusler alloys. The Born-Huang stability criteria for cubic lattices—specifically $C_{11} > |C_{12}|$, $C_{11} + 2C_{12} > 0$, and $C_{44} > 0$—are satisfied for both materials, confirming their mechanical stability and suggesting that these alloys will retain their structural integrity under a range of mechanical stresses. The pronounced difference in magnitudes between C_{11}, C_{12}, and C_{44} further indicates significant elastic anisotropy, implying that these materials are most resistant to deformation along the principal cubic axes, while shear deformation (related to C_{44}) is more easily induced along other directions.

The bulk modulus B, derived from these elastic constants, is nearly isotropic in both CoCrZrAl and RuCrZrGa, as indicated by the similarity of the computed values across different crystallographic directions. This suggests that both materials exhibit similar resistance to volumetric compression, regardless of the direction of applied stress, underscoring their relatively uniform compressibility. However, the shear modulus G

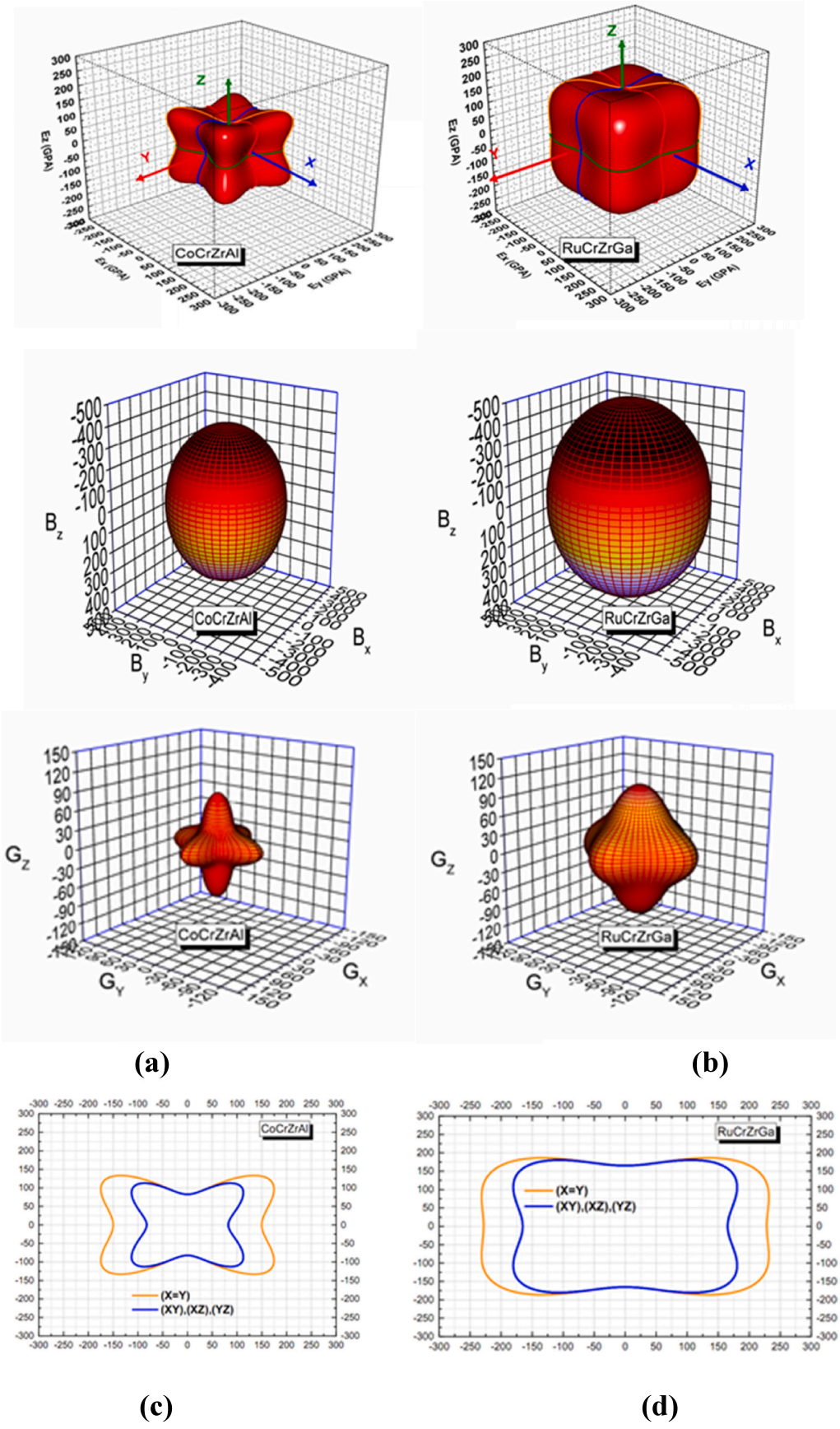

Fig. 2. Graphs of the 3D surface of the Young's modulus, bulk modulus and Shear moduli **(a)** CoCrZrAl and **(b)** RuCrZrGa **(c)** and **(d)**, the transverse sections of the Young's modulus in separated planes, respectively.

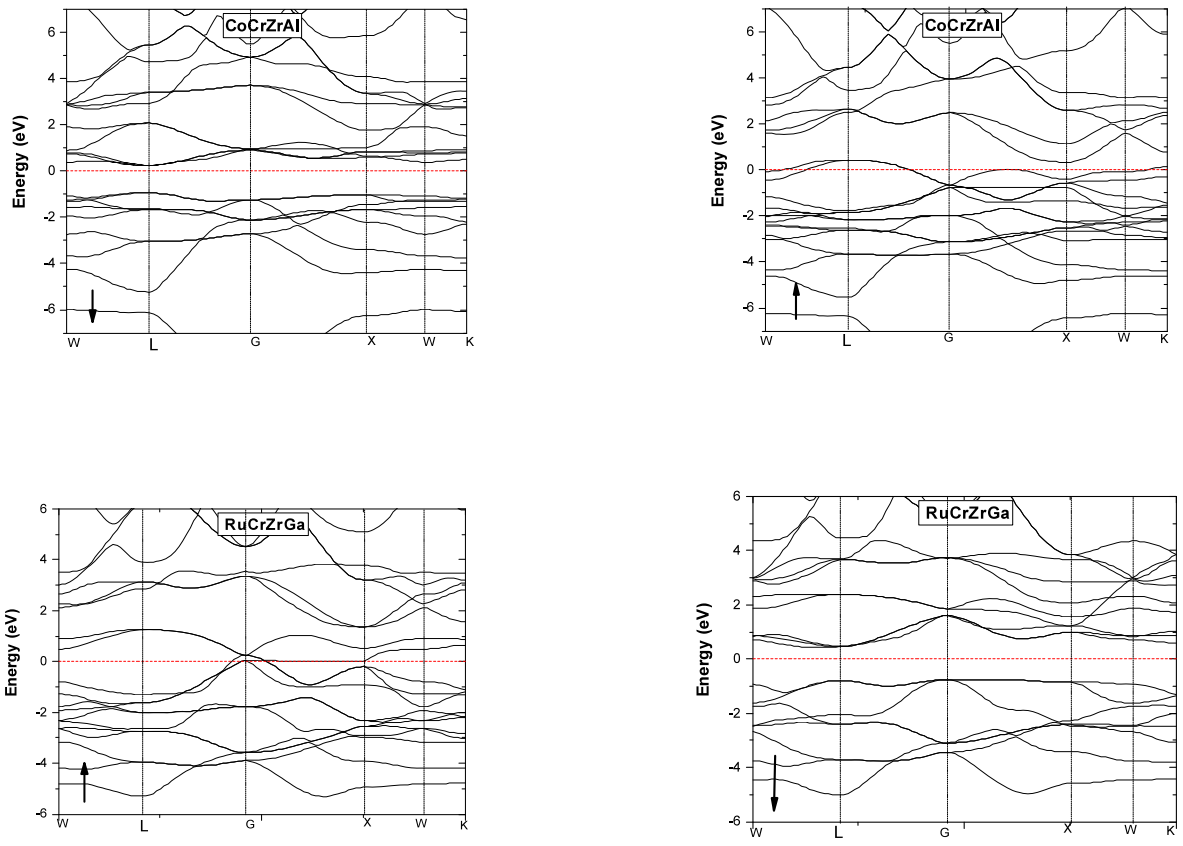

Fig. 3. Spin polarized band structure of CoCrZrAl and RuCrZrGa at their equilibrium lattice.

and C_{11} are higher for RuCrZrGa, indicating that it exhibits superior resistance to shear deformation and volumetric compression compared to CoCrZrAl. This enhanced stiffness in RuCrZrGa is attributed to the more diffuse nature of the Ru *4d* orbitals, which facilitate stronger covalent bonding, in contrast to the more localized Co *3d* orbitals in CoCrZrAl.

The directional dependence of stiffness in these alloys is comprehensively illustrated in Fig. 2, which shows the three-dimensional surfaces of Young's modulus E, bulk modulus B, and shear modulus G. While the bulk modulus remains nearly isotropic, the surfaces for Young's modulus and shear modulus exhibit distinct anisotropic characteristics. Particularly for Young's modulus, the surfaces deviate significantly from spherical symmetry, revealing well-defined "hard" and "easy" axes of deformation. These axes correspond to directions in the crystal lattice where the material is either most resistant or most susceptible to deformation. The transverse sections of Young's modulus shown in parts (c) and (d) of the figure further emphasize the pronounced elastic anisotropy in both alloys, with CoCrZrAl exhibiting more significant directional dependence than RuCrZrGa. This is reflected in the anisotropy factors A, where CoCrZrAl has a value of 1.43, indicating higher anisotropy, compared to 0.35 for RuCrZrGa, demonstrating that RuCrZrGa's mechanical properties are less directionally dependent than CoCrZrAl's.

The elastic anisotropy of both materials is quantified using the anisotropy factor A, with a value of 1 indicating perfect isotropy. While both alloys show anisotropic behavior, CoCrZrAl exhibits a much stronger directional dependence of its mechanical properties compared to RuCrZrGa. The differences in anisotropy between these two materials are visually confirmed by the distinct shapes of the surfaces for Young's modulus in Fig. 2. This anisotropy aligns with the findings of Felser and his collaborators [39], who have extensively studied the elastic behavior of Heusler alloys.

Furthermore, multiple indicators support the ductile character of both materials. Pugh's ratio B/G, which is a reliable predictor of ductility, yields values of 2.27 for CoCrZrAl and 1.91 for RuCrZrGa, both exceeding the critical threshold of 1.75 that distinguishes ductile materials from brittle ones [40]. Poisson's ratio ν, with values of 0.31 for CoCrZrAl and 0.28 for RuCrZrGa, further affirms their ductility, as both values lie well above the threshold of approximately 0.26 [41]. The positive Cauchy pressure (C_{12} - C_{44}) for both alloys indicates metallic bonding, which, according to Pettifor's criterion [42], facilitates dislocation motion and supports plastic deformation, a hallmark of ductility.

The Debye temperature θ_D, calculated from the elastic constants, is higher for RuCrZrGa, indicating that it has a stiffer lattice and higher vibrational frequencies, which is consistent with its enhanced elastic moduli.

The analysis of the elastic constants reveals that both CoCrZrAl and RuCrZrGa are mechanically stable, ductile materials with strong metallic bonding. RuCrZrGa exhibits superior overall strength and stiffness, while CoCrZrAl is characterized by greater ductility and more pronounced elastic anisotropy. The directional mechanical properties, vividly illustrated by the 3D surfaces in Fig. 2, highlight the importance of crystallographic orientation in determining the materials' mechanical behavior. The comparison of the anisotropy factors and the visual representation of the moduli emphasize that while both alloys are anisotropic, CoCrZrZrAl shows a much stronger directional dependence in its mechanical properties than RuCrZrGa, a key factor for their potential application in various engineering and functional materials contexts.

3.3. Electronic and magnetic properties

To understand the metallic, semiconducting, or semi-metallic behavior of materials and their suitability for spintronic applications, the study of electronic band structures and the corresponding density of states (DOS) is crucial. This analysis provides a detailed understanding of the material's electronic configuration, interaction dynamics, and

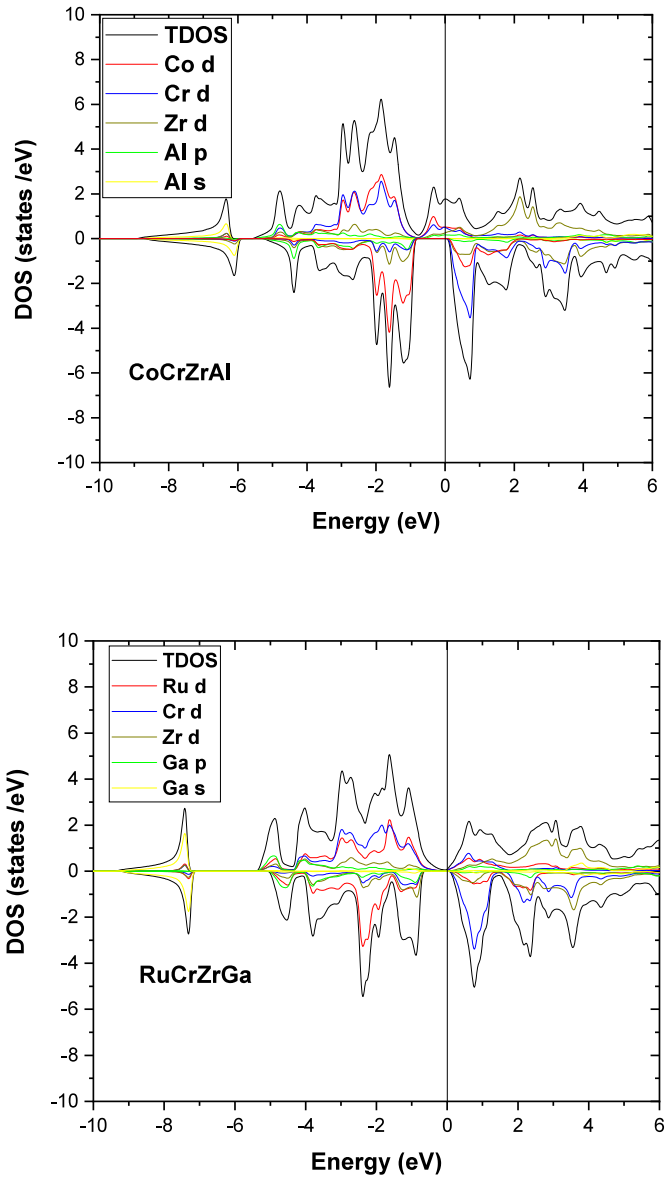

Fig. 4. The total and partial density of states of the CoCrZrAl and RuCrZrGa in type 1 calculated by GGA.

bonding characteristics. These properties are pivotal for assessing the material's ability to perform in devices requiring high spin polarization, such as spin injectors, spin valves, and other spintronic systems.

Fig. 3 presents the electronic band structures of CoCrZrAl and RuCrZrGa for both spin-up (↑) and spin-down (↓) channels. The CoCrZrAl alloy exhibits a metallic behavior in the spin-up channel, with several electronic bands crossing the Fermi level (E_F), a hallmark of metallic conductivity. In stark contrast, the spin-down channel shows a significant forbidden band around the Γ point, with an energy gap of approximately $E_g = 1.18$ eV, where no bands intersect the *Fermi* level. This indicates semiconducting properties for the spin-down channel. The disparity between the two spin channels results in a near-total spin polarization at the Fermi energy, confirming the half-metallic nature of CoCrZrAl. This spin polarization is a fundamental characteristic for spintronic devices, where the ability to inject highly spin-polarized currents is essential. The half-metallic nature of CoCrZrAl places it as a potential candidate for applications in spintronic components, such as spin injectors and spin valves, where the efficient control of electron spins is crucial.

For RuCrZrGa, as shown in Fig. 3, the band structure also reveals asymmetric behavior between the two spin channels. The spin-up channel exhibits a metallic nature, with several bands crossing the Fermi level, while the spin-down channel presents a pronounced forbidden gap ($E_g = 1.19$ eV), confirming semiconductor-like behavior for this spin orientation. This clear separation between the spin-up and spin-down channels indicates that RuCrZrGa also exhibits half-metallic characteristics, with full spin polarization at the *Fermi* energy. The material's half-metallic nature, coupled with its high spin polarization, makes it an attractive candidate for advanced spintronic devices where efficient spin filtering and manipulation are required.

To further elucidate the electronic characteristics of XCrZrZ (X = Co, Ru; Z = Al, Ga) alloys, we computed the total and partial densities of states (TDOS and PDOS), as presented in Fig. 4. These calculations, based on the generalized gradient approximation (GGA-PBESOL), reveal key insights into the electronic structure. The TDOS confirms the metallic nature of the majority spin states, which is evident from the states crossing the Fermi level in the spin-up channels. Conversely, the minority spin states exhibit semiconductor-like behavior, with the absence of states at the Fermi level in the spin-down channel. The TDOS analysis also shows that the energy range beyond [−4, 4] eV is primarily occupied by the (*s*, *p*) orbitals from the Z elements (Al, Ga), reflecting the bonding of these elements. Within the range of [−4, 4] eV, significant hybridization occurs between the 3d orbitals of the X elements (Co, Ru) and the Cr states, as well as between the *4d* orbitals of Zr and the *3d* orbitals of Cr. This hybridization plays a critical role in the material's electronic behavior, influencing both the conductivity and the spin polarization. The contribution of the *4d* orbitals of Zr is particularly important, as it further modulates the electronic structure and enhances the material's overall stability.

Magnetically, both CoCrZrAl and RuCrZrGa exhibit distinct magnetic properties, as derived from Hirshfeld electron population analysis. The magnetic moments of these materials primarily arise from the Cr atoms, consistent with the expectation for Heusler alloys. The total magnetic moments (M_t) for CoCrZrAl and RuCrZrGa are calculated to be 4 μ_B and 3 μ_B, respectively, at 0 GPa. These values are in accordance with the Slater-Pauling relation, $M_t = Z_t - 2N\downarrow$, where Zt is the total number of valence electrons per formula unit, and N↓ is the number of spin-down electrons. Specifically, for CoCrZrAl, $Z_t = 22$ and $N\downarrow = 9$, while for RuCrZrGa, $Z_t = 21$ and $N\downarrow = 9$. These computed magnetic moments are in excellent agreement with previous theoretical calculations, further confirming the validity of the predicted magnetic behavior in these materials [43]. The consistency of the magnetic moment values with the Slater-Pauling law also underscores the robustness of the half-metallic ferromagnetic characteristics, making these alloys suitable candidates for spintronic applications that rely on controlled magnetic moments and high spin polarization (see Table 4).

So, both CoCrZrAl and RuCrZrGa exhibit half-metallic behavior, with complete spin polarization at the Fermi energy, making them excellent candidates for advanced spintronic applications. Their band structures reveal metallic properties in the majority spin states and semiconducting behavior in the minority spin states, confirming their half-metallic characteristics. The detailed analysis of the DOS further highlights the hybridization between different orbital types, influencing the material's electronic properties and spin polarization. The calculated magnetic moments, consistent with the Slater-Pauling law, reinforce the suitability of these materials for applications requiring strong magnetic interactions and spin-polarized currents. These findings contribute to the growing understanding of Heusler alloys in spintronic applications, providing a foundation for future research and technological advancements in this field.

3.4. Optical properties

Optical properties describe a material's response when exposed to light. The interaction between photons and the electronic or crystal structure of a material can lead to various phenomena, offering insight

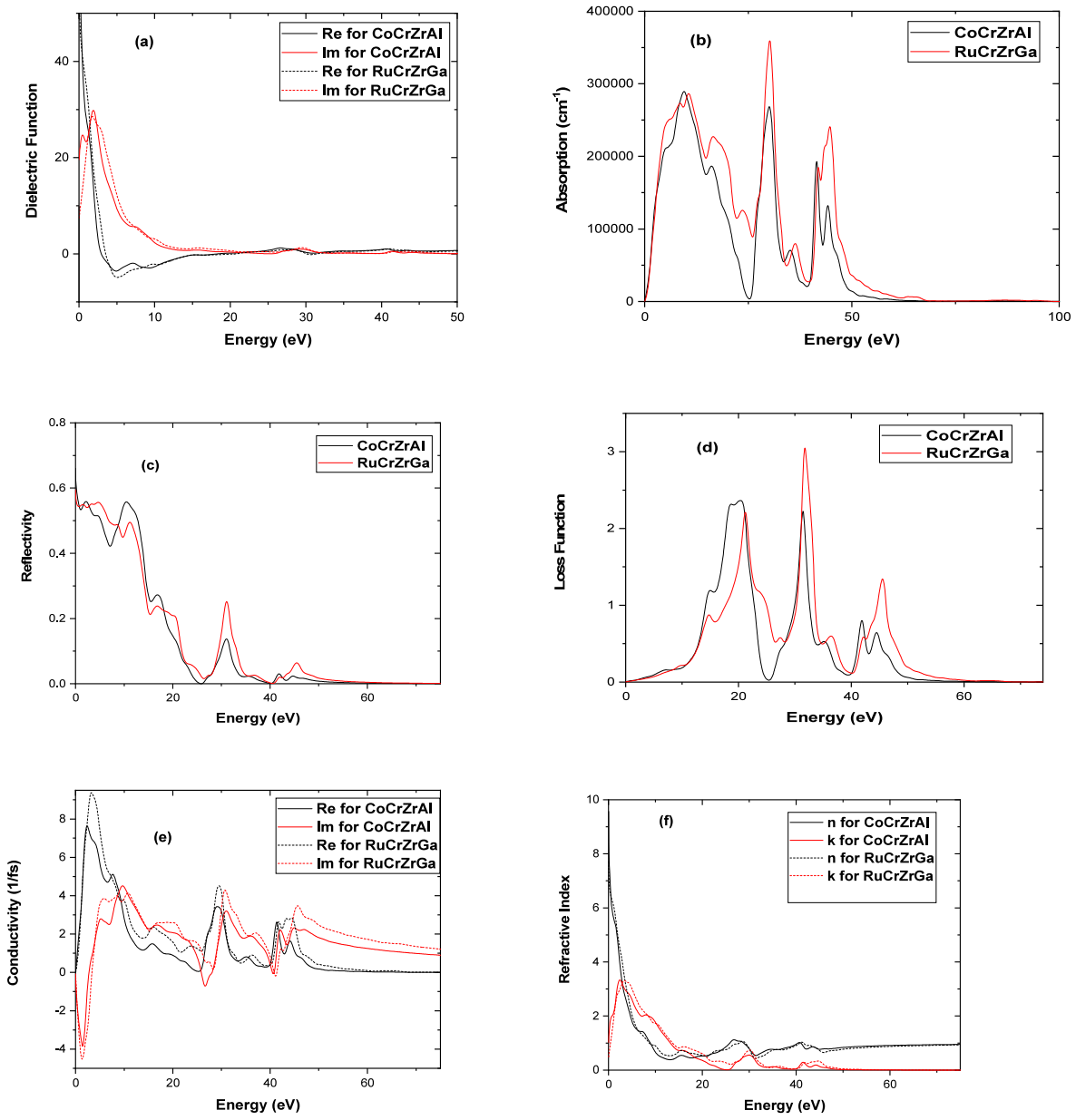

Fig. 5. (a) Dielectric function (b) absorption coefficient (c) Reflectivity spectra and (d) the energy loss L(w) (e) conductivity and (f) the refractive index as a function of energy for CoCrZrAl and RuCrZrGa.

into the material's intrinsic behavior. For CoCrZrAl and RuCrZrGa, The Generalized Gradient Approximation (GGA) was used to compute several optical properties, including the absorption coefficient (α(ω)), optical conductivity (σ(ω)), energy loss function (L(ω)), reflectivity (R (ω)), refractive index (n(ω)), and extinction coefficient (k(ω)) [44].

The optical characteristics of materials are derived from their dielectric function, ϵ(ω), which describes how the material reacts to external electromagnetic fields. This function consists of two main components: interband and intraband transitions. The dielectric function is categorized into real and imaginary components. The dielectric function can be articulated using Ehrenreich and Cohen's equation as [45,46]:

$$\varepsilon(\omega) = \varepsilon_1(\omega) + i\,\varepsilon_2(\omega) \tag{11}$$

The real part of the dielectric function, $\varepsilon_1(\omega)$, pertains to the permeability component that quantifies the energy retained within the material. The imaginary component $\varepsilon_2(\omega)$ pertains to the energy dissipation of the optical system within the medium.

Fig. 5A depicts the real and imaginary parts of dielectric function $\varepsilon(\omega)$ for both alloys derived via GGA approximation. The energy range of the study was 0–40 eV. It is worthy to note that the dielectric function includes contributions from the two spins configurations, that is, spin up and spin down. One can observe that $\varepsilon_1(\omega)$ starts from large negative values, whereas $\varepsilon_2(\omega)$ starts from large positive values at low energies for CoCrZrAl and RuCrZrGa compounds. This behavior is characteristic of intraband transitions, which arise from free electrons.

Further, regions of energy where $\varepsilon_1(\omega)$ is negative, the materials exhibit a metallic behavior and characterized by the occurrence of a high reflection. The spectral domain where the studied materials behave as metals is large (i.e., 3–17 eV). They could be used in coating or as reflectors. The transition frequency from negative to positive values of $\varepsilon_1(\omega)$ is called plasmon frequency. The plasmon frequency is always correlated to the free electron density in materials [47–50].

The computed static real dielectric constants $\varepsilon_1(0)$ for CoCrZrAl and RuCrZrGa are 84 and 59, respectively.

At $\omega = 0$ eV, the values of ε_2 (the imaginary component of the

dielectric function) for CoCrZrAl and RuCrZrGa are roughly 19.74 and 8.16 arbitrary units, respectively. This indicates that both materials possess non-zero absorption coefficients at zero photon energy, signifying intrinsic electronic transitions or excitations.

Furthermore, $\varepsilon_2(\omega)$ attains its peak value in the infrared range and diminishes to zero in the ultraviolet zone.

The absorption coefficient provides information on the optimal solar energy transformation efficiency. The optical absorption $\alpha(\omega)$ shown in Fig. 5b demonstrates the significant photon energy absorption in the range (0–50) eV with three remarkedly high peaks at about 9, 30 and 44 eV. This identifies the optically active zone of the current materials. One can notice that the absorption coefficient at the prominent peaks reaches very high values of 3×10^5 cm^{-1}. More importantly, the absorption coefficient in the visible range is well above 10^5 cm^{-1}, These high absorption values make these materials attractive for solar cells applications.

Fig. 5f illustrates the refractive index. The refractive index is 9.56 for CoCrZrAl and 7.70 for RuCrZrGa, both of which diminish with increasing photon energy. The energy loss function, or bulk plasma frequency (ω_p), is characterized by the peak occurring when the imaginary component of the dielectric function is negative, while the real component approaches zero (Fig. 5d). The maxima of the energy loss function are situated at approximately 20 eV for both substances. Fig. 5e illustrates conductivity (σ) resulting from photon absorption. The initial peak of optical conductivity is situated in the visible spectrum, whereas the most pronounced peak occurs in the ultraviolet region, signifying that CoCrZrAl and RuCrZrGa exhibit photoconductivity in both the visible and ultraviolet domains. The acceptable value of σ in the visible spectrum indicates that this alloy possesses potential for solar cell applications [51,52].

4. Conclusion

In summary, a detailed DFT-based investigation of CoCrZrAl and RuCrZrGa quaternary Heusler alloys has been conducted. The negative formation energies and satisfaction of the Born-Huang stability criteria affirm the compounds' thermodynamic and mechanical stability. Both alloys are identified as half-metallic ferromagnets, achieving perfect 100 % spin polarization with substantial band gaps in the minority spin channel. Their total magnetic moments strictly adhere to the Slater-Pauling rule, with the Cr atom being the primary contributor. Elastic constants and moduli reveal that both materials are ductile, with RuCrZrGa exhibiting greater stiffness and CoCrZrAl showing higher elastic anisotropy. The optical analysis demonstrates strong absorption in the visible and ultraviolet spectrum, alongside high reflectivity in certain energy ranges. The confluence of robust half-metallicity, ductility, and favorable optical characteristics underscores the significant potential of CoCrZrAl and RuCrZrGa for applications in next-generation spintronics, such as spin injectors and tunnel junctions, as well as in optoelectronic devices like solar cells and UV photodetectors.

CRediT authorship contribution statement

I. Bensehil: Writing – review & editing, Writing – original draft, Investigation, Data curation, Conceptualization. **H. Baaziz:** Writing – review & editing, Writing – original draft, Supervision, Software, Methodology, Investigation, Formal analysis. **T. Ghellab:** Writing – review & editing, Writing – original draft, Software, Data curation, Conceptualization. **Z. Charifi:** Writing – review & editing, Validation, Resources, Investigation, Formal analysis.

Declaration of competing interest

The authors declare that they have no known competing financial interests or personal relationships that could have appeared to influence the work reported in this paper.

Acknowledgments

The authors would like to thank the general directorate for scientific research and technological development for their financial support during the realization of this work.

Data availability

Data will be made available on request.

References

[1] R.A. De Groot, F.M. Mueller, P.G.V. Engen, K.H.J. Buschow, New class of materials: half-metallic ferromagnets, Phys. Rev. Lett. 50 (25) (1983) 2024–2027, https://doi.org/10.1103/PhysRevLett.50.2024.
[2] I.H. Bhat, S. Yousuf, T. Mohiuddin Bhat, D.C. Gupta, Investigation of electronic structure, magnetic and transport properties of half-metallic Mn2CuSi and Mn2ZnSi Heusler alloys, J. Magn. Magn Mater. 395 (2015) 81–88, https://doi.org/10.1016/J.JMMM.2015.07.022.
[3] T. Dietl, H. Ohno, F. Matsukura, J. Cibert, D. Ferrand, Zener model description of ferromagnetism in zinc-blende magnetic semiconductors, Science 287 (5455) (2000) 1019–1022, https://doi.org/10.1126/science.287.5455.1019.
[4] K.-I. Kobayashi, T. Kimura, H. Sawada, K. Terakura, Y. Tokura, Room-temperature magnetoresistance in an oxide material with an ordered double-perovskite structure, Nature 395 (6703) (1998) 677–680, https://doi.org/10.1038/27132.
[5] I. Galanakis, P.H. Dederichs, N. Papanikolaou, Slater-Pauling behavior and origin of the half-metallicity of the full-Heusler alloys, Phys. Rev. B 66 (17) (2006) 174429, https://doi.org/10.1103/PhysRevB.66.174429.
[6] T. Graf, C. Felser, S.S.P. Parkin, Simple rules for the understanding of Heusler compounds, Prog. Solid State Chem. 39 (1) (2011) 1–50.
[7] C. Felser, G.H. Fecher, B. Balke, Spintronics: a challenge for materials science and solid-state chemistry, Angew. Chem. Int. Ed. 46 (5) (2007) 668–699.
[8] I. Galanakis, P. Mavropoulos, Spin polarization and electronic structure of half-metallic Heusler alloys calculated from first principles, J. Phys. Condens. Matter 19 (31) (2007) 315213.
[9] S. Ouardi, G.H. Fecher, C. Felser, J. Kübler, Realization of spin gapless semiconductors: the Heusler compound Mn2CoAl, Phys. Rev. Lett. 110 (10) (2013) 100401.
[10] G. Kresse, J. Furthmüller, Efficient iterative schemes for ab initio total-energy calculations using a plane-wave basis set, Phys. Rev. B 54 (16) (1996) 11169.
[11] J.P. Perdew, K. Burke, M. Ernzerhof, Generalized gradient approximation made simple, Phys. Rev. Lett. 77 (18) (1996) 3865–3868.
[12] R. Prakash, G. Kalpana, DFT investigation of half-metallic, thermoelectric and optical properties of MCrTaM' (M = Fe and Ru, M' = Al, Ga, Si and Ge) quaternary-Heusler alloys, J. Mater. Sci. 60 (2025) 3830–3849, https://doi.org/10.1007/s10853-025-10678-z.
[13] A.Q. Seh, D.C. Gupta, Quaternary Heusler alloys a future perspective for revolutionizing conventional semiconductor technology, J. Alloys Compd. 871 (2021) 159560, https://doi.org/10.1016/j.jallcom.2021.159560.
[14] R. Prakash, G. Suganya, G. Kalpana, Investigation of novel quaternary Heusler alloys XRuCrZ (X = Co, Ni, Rh, and Pd; Z = Si and Ge) via first-principles calculation for spintronics and thermoelectric applications, AIP Adv. 12 (2022) 055223, https://doi.org/10.1063/5.0088553.
[15] Deepika Rani, Lakhan Bainsla, K.G. Suresh, Aftab Alam, experimental and theoretical investigation on the possible half-metallic behaviour of equiatomic quaternary Heusler alloys: corumnge and CoRuVZ (Z = Al, Ga), J. Magn. Magn Mater. 492 (2019) 165662, https://doi.org/10.1016/j.jmmm.2019.165662.
[16] Z. Khadhraoui, S.E. Amara, A.Y. Behlali, H. Kheribot, S. Makhlouf, S. Labidi, et al., Comprehensive analysis: exploring quaternary Heusler alloys CoFeXGe (X = Hf and Ta) through first-principles calculations, J. Am. Ceram. Soc. 107 (2024) 7421–7440, https://doi.org/10.1111/jace.20014.
[17] H.A. Masri, M.S. Abu-Jafar, A. Bouhemadou, N. Baadji, [Multifunctional Properties of FeMnScAl Quaternary Heusler Alloy: Insights into Spintronics, Photovoltaics, and Thermoelectric Applications], J. Phys. Chem. C 129 (5) (2025) 2672–2690, https://doi.org/10.1021/acs.jpcc.4c06553.
[18] R. Prakash, G. Kalpana, First-principles study on novel Fe-based quaternary Heusler alloys, with robust half-metallic, thermoelectric and optical properties, RSC Adv. 13 (16) (2023) 10847–10860, https://doi.org/10.1039/d3ra00942d.
[19] X.-P. Wei, T.-Y. Cao, X.-W. Sun, Q. Gao, P.-F. Gao, Z.-L. Gao, X.-M. Tao, Structural, electronic, and magnetic properties of quaternary Heusler CrZrCoZ compounds: a first-principles study, Chin. Phys. B 29 (7) (2020) 077105, https://doi.org/10.1088/1674-1056/ab969b.
[20] Ghellab,T. , Baaziz, Charifi,Z., H., Tailoring the physical characteristics of novel quaternary RuMnCrSi and NiMnCrAl compounds for spintronic and thermoelectric applications. Phys. Scri., 100(5). https://doi.org/10.1088/1402-4896/adc855.
[21] Y. Venkateswara, J. Nag, S.S. Samatham, A.K. Patel, P.D. Babu, M.R. Varma, J. Nayak, K.G. Suresh, A. Alam, FeRhCrSi: spin semimetal with spin-valve behavior at room temperature, Phys. Rev. B 107 (10) (2023) L100401, https://doi.org/10.1103/PhysRevB.107.L100401.
[22] H. Alqurashi, R. Haleoot, B. Hamad, First-principles investigations of the electronic, magnetic and thermoelectric properties of VTiRhZ (Z = Al, Ga, In)

quaternary Heusler alloys, Mater. Chem. Phys. 278 (2021) 125685, https://doi.org/10.1016/j.matchemphys.2021.125685.
[23] Z. Khadhraoui, S.E. Amara, A.Y. Behlali, H. Kheribot, S. Makhlouf, S. Labidi, A. Amara, Comprehensive analysis: exploring quaternary Heusler alloys CoFeXGe (X = Hf and Ta) through first-principles calculations, J. Am. Ceram. Soc. 107 (11) (2024) 7421–7440, https://doi.org/10.1111/jace.20014.
[24] K. Bouferrache, M.A. Ghebouli, B. Ghebouli, M. Fatmi, S. Alomairy, T. Chihi, Stability, electronic band structure, magnetic, optical and thermoelectric properties of CoXCrZ (X = Fe, Mn and Z = Al, Si) and FeMnCrSb quaternary Heusler alloys, Chin. J. Phys. 81 (2022) 303–324, https://doi.org/10.1016/j.cjph.2022.10.003.
[25] I. Bensehil, H. Baaziz, T. Ghellab, et al., Investigating the structural, electronic, magnetic, mechanical, anisotropic and optical aspects of CoFeYSb (Y = V and ti) Quaternary heusler alloys from first principles, J. Supercond. Nov. Magnetism 38 (2025) 59, https://doi.org/10.1007/s10948-024-06898-0.
[26] R. Mahabubur, Molly De Raychaudhury, Enhanced ferromagnetism in half-metallic CoIrZrAl quaternary Heusler alloy: a density functional study, Mater. Chem. Phys. 340 (2025) 130808, https://doi.org/10.1016/j.matchemphys.2025.130808.
[27] I. Bensehil, H. Baaziz, T. Ghellab, Z. Charifi, A. Kolli, N. Guechi, Electronic, magnetic, and elastic features of Quaternary heusler alloys: Fevscsb and FeVYSb, Phys. Status Solidi B 260 (2023) 2300178, https://doi.org/10.1002/pssb.202300178.
[28] Y. Wang, Z. Xiaoming, B. Dinga, H. Houa, E. Liua, L. Zhongyuan, X. Xia, H. Zhanga, G. Wua, W. Wanga, Comput. Mater. Sci. 150 (2018) 321.
[29] A. Kolli, N. Guechi, M. Kharoubi, A. Kharmouche, First-principles characterization of structural, elastic, electronic phase transitions and magnetic properties of FeCrScZ (Z = Si, Ge) Heusler compounds under pressure, Phys. B Condens. Matter 673 (2024) 415498, https://doi.org/10.1016/j.physb.2023.415498.
[30] M.C. Payne, M.P. Teter, D.C. Allan, T.A. Arias, J.D. Joannopoulos, Iterative minimization techniques for ab initio total-energy calculations: molecular dynamics and conjugate gradients, Rev. Mod. Phys. 64 (1992) 1045–1097, https://doi.org/10.1103/RevModPhys.64.1045.
[31] M.D. Segall, P.J. Lindan, M.A. Probert, C.J. Pickard, P.J. Hasnip, S.J. Clark, M. C. Payne, First principles simulation: ideas, illustrations and the CASTEP code, J. Phys. Condens. Matter 14 (2002) 2717–2744, https://doi.org/10.1088/0953-8984/14/11/301.
[32] J.P. Perdew, K. Burke, M. Ernzerhof, Generalized gradient approximation made simple, Phys. Rev. Lett. 77 (1996) 3865–3868, https://doi.org/10.1103/PhysRevLett.77.3865.
[33] D. Vanderbilt, Soft self-consistent pseudopotentials in a generalized eigenvalue formalism, Phys. Rev. B 41 (1990) 7892–7895, https://doi.org/10.1103/PhysRevB.41.7892.
[34] J.F. Nye, Physical Properties of Crystals: Their Representation by Tensors and Matrices, Oxford university press, Oxford, 1985.
[35] T. Katsura, Y. Tange, A simple derivation of the birch–murnaghan equations of state (EOSs) and comparison with EOSs derived from other definitions of finite strain, Minerals 9 (2019) 745.
[36] B.R. Sahu, Electronic structure and bonding of ultralight LiMg, Mater. Sci. Eng. B49 (1997) 74–78, https://doi.org/10.1016/S0921-5107(97)00068-8.
[37] M. Born, K. Huang, Dynamical Theory of Crystal Lattices, Clarendon, Oxford, 1956.
[38] M. Jamal, S. Jalali Asadabadi, I. Ahmad, H.A. Rahnamaye Aliabad, Comput. Mater. Sci. 95 (2014) 592.
[39] S. Wu, S.S. Naghavi, G.H. Fecher, C. Felser, A critical study of the elastic properties and stability of Heusler compounds: cubic Co_2YZ compounds with L_{21} structure, J. Appl. Phys. 125 (8) (2017) 082523, https://doi.org/10.1063/1.5054398.
[40] S.F. Pugh XCII, Relations between the elastic moduli and the plastic properties of polycrystalline pure metals, London, Edinburgh Dublin Phil. Mag. J. Sci. 45 (367) (1954) 823–843, https://doi.org/10.1080/14786440808520496.
[41] M. Mushtaq, M.A. Sattar, S.A. Dar, Phonon phase stability, structural, mechanical, electronic, and thermoelectric properties of two new semiconducting quaternary Heusler alloys <scp>CoCuZrZ</scp> (Z = Ge and Sn), Int. J. Energy Res. 44 (2020) 5936–5946, https://doi.org/10.1002/er.5373.
[42] D.G. Pettifor, Theoretical predictions of structure and related properties of intermetallics, Mater. Sci. Technol. 8 (4) (1992) 345–349, https://doi.org/10.1179/MST.1992.8.4.345.
[43] S. Nepal, R. Dhakal, I. Galanakis, S.M. Winter, R.P. Adhikari, G.C. Kaphle, Ab-initio study of stable 3d, 4d and 5d transition metal based Quaternary Heusler compounds, Phys. Rev. Mater. 6 (11) (2022) 114407, https://doi.org/10.1103/PhysRevMaterials.6.114407.
[44] Moaid K. Hussain, B.J. Kahdum, R. Paudel, S. Syrotyuk, Electron, Mater 52 (2023) 258–269, https://doi.org/10.1007/s11664-022-09981-1.
[45] J. Petzelt, I. Rychetský, Dielectric function, in: F. Bassani, G.L. Liedl, P. Wyder (Eds.), Encyclopedia of Condensed Matter Physics, Elsevier, Oxford, 2005, pp. 426–429, https://doi.org/10.1016/B0-12-369401-9/00427-7.
[46] P. Hofmann, *Solid State Physics*: an Introduction, Wiley, Hoboken, 2022.
[47] H. Baaziz, T. Ghellab, E. Güler, et al., Investigating the magnetic, mechanical, electronic, optical, and anisotropic properties of ZrCoFeX (X = Si, Ge) Quaternary heusler alloys via first principles, J. Supercond. Nov. Magnetism 35 (2022) 1173–1182, https://doi.org/10.1007/s10948-022-06155-2.
[48] H. Ammi, Z. Charifi, H. Baaziz, T. Ghellab, L. Bouhdjer, S. Adalla, H.Y. Ocak, Ş. Uğur, G. Uğur, Investigation on the hydrogen storage properties, electronic, elastic, and thermodynamic of Zintl phase hydrides XGaSiH (X = sr, ca, ba), Int. J. Hydrogen Energy 87 (2024) 966–984, https://doi.org/10.1016/j.ijhydene.2024.09.087.
[49] T. Ghellab, H. Baaziz, Z. Charifi, H. Latelli, Mais Jamil A. Ahmad, Mahmoud Telfah, Ahmad Alsaad, Ahmad Telfah, Roland Hergenröder, Renat Sabirianov, First-principles calculations of the high-pressure behavior, electronic, magnetic, and elastic properties of praseodymium pnictides: PrX (X = P, as and Bi), J. Magn. Magn Mater. 546 (2022) 168919, https://doi.org/10.1016/j.jmmm.2021.168919.
[50] I. Bensehil, H. Baaziz, T. Ghellab, et al., Investigating the structural, electronic, magnetic, mechanical, anisotropic and optical aspects of CoFeYSb (Y = V and ti) Quaternary heusler alloys from first principles, J. Supercond. Nov. Magnetism 38 (2025) 59, https://doi.org/10.1007/s10948-024-06898-0.
[51] N. Belmiloud, F. Boutaiba, A. Belabbes, M. Ferhat, F. Bechstedt, Half-Heusler compounds with a 1eV (1.7eV) direct band gap, lattice-matched to GaAs (Si), for solar cell application: a first-principles study, Physica Status Solidi (B) Basic Research. 253 (2016) 889–894, https://doi.org/10.1002/pssb.201552674.
[52] D. Kieven, R. Klenk, S. Naghavi, C. Felser, T. Gruhn, I-II-V half-Heusler Compounds for Optoelectronics: Ab Initio Calculations, 2010, pp. 1–6, https://doi.org/10.1103/PhysRevB.81.075208.